Direct control of magnetic chirality in $NdMn_2O_5$ by external electric field

I.A. Zobkalo,[1] A.N. Matveeva,[1] A. Sazonov,[2] S.N. Barilo,[3] S.V. Shiryaev,[3] B. Pedersen,[4] V. Hutanu[2]

[1]*B.P Konstantinov Petersburg Nuclear Physics Institute, Kurchatov Institute, Gatchina, 188300, Russia;*
[2]*Institute of Crystallography, RWTH Aachen University and Jülich Centre for Neutron Science (JCNS) at Heinz Maier- Leibnitz Zentrum (MLZ), 85747 Garching, Germany;*
[3]*Scientific-Practical Materials Research Centre NAS of Belarus, 19 P. Brovki str., Minsk, 220072, Belarus;*
[4]*Heinz Maier- Leibnitz Zentrum (MLZ), Technische Universität München, Lichtenbergstr. 1, 85748 Garching, Germany.*

Detailed investigation of the incommensurate magnetic ordering in single crystal of multiferroic $NdMn_2O_5$ has been performed using both non-polarized and polarized neutron diffraction techniques. Below $T_N \approx 30.5$ K magnetic Bragg reflections corresponding to the non-chiral type magnetic structure with propagation vector $\boldsymbol{kz_1} = (0.5\ 0\ k_{z1})$ occurs. Below about 27 K a new distorted magnetic modulation with similar vector kz2 occurs, this was attributed to the magnetization of the Nd ions by the Mn-sub-lattice. Strong temperature hysteresis in the occurrence of the incommensurate magnetic phases in $NdMn_2O_5$ was observed depending on the cooling or heating history of the sample. Below about 20 K magnetic structure became of chiral type. From spherical neutron polarimetry measurements the resulting low-temperature magnetic structure kz3 was approximated by general elliptic helix. The parameter of the magnetic helix like ellipticity and helical plane orientation in regard to the crystal structure were determined. A reorientation of the helix occurs at an intermediate temperature between 4 K and 18 K. A difference between the population of right- and left-handedness chiral domains of about 0.2 were observed in the as-grown crystal when cooling without an external electric field. The chiral magnetic ratio can be changed by the application of external electric field of few kV/cm, revealing strong magnetoelectric coupling. A linear dependence of the magnetic chirality on the applied electric field in $NdMn_2O_5$ was found. The results are discussed within the frame of antisymmetric super-exchange model for Dzyaloshinsky-Moria interaction.

I. INTRODUCTION

Magnetic multiferroics have attracted an increasing scientific interest in the last one and half decades. In this class of materials magnetic order induces the long range polar order and vice versa, thus both order parameters are strongly coupled. A coupling between the two ferroic orders can induce novel functional properties that do not exist in either state alone. This fact provides technological interest to such materials, in particular of their potential use in various areas of spintronics, but also from the fundamental understanding of various microscopic mechanisms leading to the magneto-electric coupling.

Manganite oxides family RMn_2O_5 (R – rare-earth element) represents prominent example of a multiferroics with extremely interesting and close relationship between magnetism and ferroelectricity [1-3], including a magnetically induced polarization flop in $TmMn_2O_5$ [4], a polarization flip in $TbMn_2O_5$, also induced by a magnetic field [1], or electrically induced switching of antiferromagnetic domains in YMn_2O_5 [5]. The temperature evolution of the

magnetic structure of multiferroic RMn_2O_5 is rather complex, which, in the combination with a variety of magnetoelectric phenomena, makes these compounds extremely attractive from the standpoint of studying fundamental phenomena of interaction between different order parameters. The intriguing feature of the RMn_2O_5 family is that compounds with rare earth ions having radius smaller than that of Nd^{3+} are multiferroics, while those with larger radius – are not. $NdMn_2O_5$ itself, long time considered to be non-multiferroic, is of particular interest as a "border stone" in this line. Especially, only recently observed emerging of the electrical polarization in magnetically ordered phase of this compound and its much lower value compared to that in another RMn_2O_5 multiferroics [6], makes it an attractive candidate to check different proposed mechanisms of multiferroicity in this type of materials.

Generally, all member of RMn_2O_5 family are considered to be isostructural within the orthorhombic centrosymmetric space group *Pbam* [7]. This structure consists of octahedra $Mn^{4+}O_6$ edge-shared along the *c* axis and pairs of tetragonal pyramids $Mn^{3+}O_5$ linking with two $Mn^{4+}O_6$ chains. However, there are some indications in the literature about the symmetry lowering in RMn_2O_5 from *Pbam* down to $Pb2_1m$ polar group at low temperatures [8-10]. It was reported also, that in fact the structure is non-centrosymmetric even at room temperature, and non-centrosymmetric monoclinic space group *Pm* ($\gamma = 90°$) was proposed rather than centrosymmetric one *Pbam* [11]. In this structure, there are several nearly equivalent superexchange paths between manganese ions that leads to the essential exchange competition, which results in turn, in non-collinear magnetic structures and complex magnetic phases [12]. Multiple magnetic ordered phases assume sophisticated magnetic interaction schemes, so it is reasonable to suppose that several mechanisms could be responsible for complicated magneto-electrical behavior in RMn_2O_5 compounds.

The magnetic order in $NdMn_2O_5$ single crystal was studied recently by the neutron scattering [6, 13, 14]. It was found that magnetic ordering in this compound has features different from those known for other RMn_2O_5 multiferroics with smaller ion radii. For $NdMn_2O_5$ the onset of the long-range magnetic order with incommensurate wave vector $\boldsymbol{k}$ = (0.5 0 ~0.36) is observed at $T_N \approx 30$ K, while for another RMn_2O_5 multiferroics the transition to magnetically ordered phase takes place at temperatures higher than 40 K. Below 30 K two magnetic phases were reported with propagation vectors close to each other: $\boldsymbol{k_1}$ = (0.5 0 k_{z1}), $\boldsymbol{k_2}$ = (0.5 0 k_{z2}). In Refs [6, 14] it is shown that two propagation vectors merge together at temperature below T = 15 K, while in [13] we show that k_{z1}, k_{z2} components remain separated and increase monotonously with temperature decrease down to 25 K, then remain constant with values k_{z1} = 0.384(2), k_{z2} = 0.395(2). Two additional transitions were observed at ~ 20 K and at ~ 5 K. The latter is connected with Nd^{3+} subsystem alignment with $\boldsymbol{k_{Nd}}$ = (0.5 0 0) [14]. The transition at 20 K, related to the ordering of Mn magnetic moments, is of another nature and is of particular interest, since at 20 K the onset of electric polarization in $NdMn_2O_5$ single crystal was observed [6]. The most significant issue in the studies of RMn_2O_5 is the understanding of the microscopic mechanism responsible for spin-driven ferroelectricity in these compounds. The model of inverse Dzyaloshinsky-Moriya interaction (DMI) works well for magnetic multiferroics in the $RMnO_3$ family, like $TbMnO_3$, $DyMnO_3$. In this model DMI favors the displacement of O^{2-} ions, which enhances the DMI exchange interaction between non-collinearly ordered spins and breaks the inversion symmetry [15, 16]. It is important to note that in RMn_2O_5 multiferroics ferroelectric polarization enhanced in the commensurate magnetic phases with magnetic moments close to collinear alignment [2, 17]. This provides considerable difficulty in the explanation of the origin of ferroelectric polarization by the inverse DM model. In connection with this, exchange striction mechanism is used to explain the origin of ferroelectricity [10, 12]. This model refers to collinear spin orders where symmetric exchange striction forces the two nearest ions with parallel spins to move closer each other while those with antiparallel spins

to move farther. The application of this model to RMn_2O_5 seems to be reasonable since antisymmetric exchange is associated with a rather weak spin-orbit coupling. However, from another point of view, the competition of superexchange interactions leads to an exchange frustrated structure [3], and in such case, a weak antisymmetric interaction can have a significant impact on the magnetic properties and subsequently on the electric properties of such system. Apparently, this magnetic frustration is the reason why a considerable number of experimental facts indicate that a significant contribution to a rich set of magnetic phenomena in RMn_2O_5 is arising due to DMI [18, 19]. There are a number of arguments also in favor of multiple microscopic mechanisms of magnetically induced ferroelectricity in RMn_2O_5 compounds. $NdMn_2O_5$ is an ideal compound of such a study as it belongs to the same multiferroic family on the one side, but do not show a commensurate magnetic order on the other. In non-collinear incommensurate magnetic structures of DMI origin, the direction of spin rotation is fixed by DMI, while in centrosymmetric systems the magnetic energy is independent of the sense of rotation [20]. In order to clarify the role of DMI in formation of magnetic and magneto-electric properties in RMn_2O_5 we performed investigations of magnetic chirality and its evolution with the temperature and applied electric field in $NdMn_2O_5$. For that we employed the polarized neutrons diffraction. It provides great sensitivity to the direction of the spin rotation in the magnetic structure and allows to obtain information, inaccessible by other experimental techniques.

II. EXPERIMENTAL DETAILS

Single crystals of $NdMn_2O_5$ were grown by the flux-melt method described in [21]. The crystal thoroughly characterized in the previous neutron diffraction investigation [13] was used for the actual experiments. The approximate dimensions of the used sample is 3x4x5 mm^3 with longest dimension along c-axis.

The measurements for the crystal structure refinement were performed at diffractometer RESI at FRM-II reactor (Heinz Maier-Leibnitz Zentrum, Garching, Germany, MLZ) [22] using neutron wavelength of 1.039 Å. Data collection was made with position sensitive 2D detector MAR345. The 2D data reduction was performed using the the EVAL-14 suite [23].

Magnetic neutron studies were performed at diffractometer POLI at MLZ [23, 24], which permits measurements both in unpolarized and polarized diffraction modes using the same neutron wavelength. Non-polarized diffraction using variably double-focused Si (311) monochromator and wavelength of 1.15 Å, resulting in high intensity neutron flux of more than 10^7 $n(cm^2s)^{-1}$ with high resolution, was employed in order to study the thermal evolution of the magnetic Bragg reflections in $NdMn_2O_5$.

For the polarized neutron diffraction we used the technique of Spherical Neutron Polarimetry (SNP). It is implemented on POLI using third generation zero-field Cryogenic Polarization Analysis Device CRYOPAD [25]. Both neutron polarization and analysis are produced using ^3He spin filters. Such configuration is very efficient for short wavelength neutrons from the point of view of a good resolution and a high flux of the polarized neutrons on the sample position, superior to the previous investigations. At the same time the polarizing (analyzing) efficiency of the filters relaxes (decrease) with time, representing a main drawback of the technique, since additional corrections should be done to the data, which may lead to some decrease of the statistical accuracy of the measurement. The corrections were performed according to calculations described in Ref. [26]. Standard SNP axis convention was applied for the polarization analysis: ***x***-direction coincides with the scattering vector ***q***, ***y***-direction lies in the scattering plane and is perpendicular to ***x*** and ***z***-axis is oriented vertically, thus forming right-handed Cartesian coordinate system.

During the experiment with polarized neutrons the crystal *b*-axis was oriented vertically, *a* and *c* axes were laying in horizontal scattering plane. In this way the magnetic satellites of type $\boldsymbol{k} = (k_x\ 0\ k_z)$ can be reached. For the measurements with electric field crystal was mounted on sample rod of the cryostat, between the electrodes built from aluminum plates as shown in Fig. 1. The electric field was applied in vertical direction along *b*-axis. The sample was placed into a standard FRM-II type top-loading cryostat. The essentials of measurements with high electric fields in cryogenic environments consist in fine-tuning the pressure of helium exchange gas continuously on a thin line where it is possible to apply several kV/mm without electric breakdown maintaining at the same time necessary temperature control of the sample. A reliable setup for in-situ pressure control and regulation within cryostat has been developed and calibrated before starting the experiment. In this way, an electric voltage up to 5 kV (corresponding to max. 12.5 kV/cm electric field in the sample) could be applied during the experiment without electric breakdown. Power supply device FUG HCB 20M-1000 has been used for high voltage generation and high precision digital multimeter FLUKE 8846A for the current monitoring in order to avoid the breakdowns.

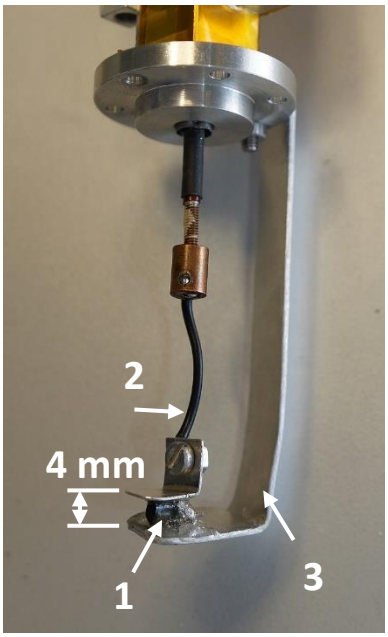

Figure 1: $NdMn_2O_5$ single crystal sample (1) between two Al electrodes; (2) – isolated high voltage contact and (3) – ground; on the sample rod of FRM II close cycle refrigerator able to control temperature between 3.8 - 325 K with the precision of better than 0.01 K.

III. EXPERIMENTAL RESULTS

A. Crystal structure refinement

For the crystal structure refinement, the datasets collections were performed at three temperatures – 300 K, 24 K, 6 K. The observed nuclear reflections were successfully indexed in *Pbam* space group and we didn't observe superstructure reflections, that should indicate that crystal symmetry is lower than *Pbam*. But we also can suppose that this could be connected with the extremely low intensity of those reflections, as it was observed in [11]. The structural refinement then was performed with FullProff suite software [27]. The results obtained within *Pbam* space group are in good agreement with those reported previously at 300 K [6, 7] and are presented at Table I. The same datasets were then used for the refinement within *Pm* space group, but the enhancement of the fit quality was negligible small by the significant increasing number of fitting parameter, which does not permit us to make the definite decision in favor of lower symmetry group.

Table I. Crystal structure parameters obtained within *Pbam* space group

300 K (a =7.4940 Å, b = 8.6071 Å, c = 5.6934 Å)			
Atom	*X*	*Y*	*Z*
Nd	0.1421(3)	0.1732(4)	0
Mn^{4+}	0	0.5	0.2556(8)
Mn^{3+}	0.4114(7)	0.3539(7)	0.5
O1	0	0	0.2717(5)
O2	0.1579(5)	0.4482(6)	0
O3	0.1520(5)	0.4366(5)	0.5
O4	0.4023(3)	0.2070(4)	0.2497(4)
24 K (a =7.4871 Å, b = 8.6293 Å, c = 5.7083 Å)			
Nd	0.1424(6)	0.1724(5)	0
Mn^{4+}	0	0.5	0.257(1)
Mn^{3+}	0.411(1)	0.354(1)	0.5
O1	0	0	0.276(1)
O2	0.1588(8)	0.4482(6)	0
O3	0.1514(8)	0.4366(6)	0.5
O4	0.4040(5)	0.2050(5)	0.2485(7)
6 K (a =7.5135 Å, b = 8.6328 Å, c = 5.7320 Å)			
Nd	0.1436(7)	0.1722(6)	0
Mn^{4+}	0	0.5	0.255(1)
Mn^{3+}	0.413(1)	0.355(1)	0.5
O1	0	0	0.277(1)
O2	0.161(1)	0.4501(7)	0
O3	0.1507(9)	0.4353(7)	0.5
O4	0.4038(6)	0.2059(5)	0.2483(9)

B. Temperature evolution of the magnetic order by non-polarized neutron diffraction

In order to identify the magnetic Bragg reflections from different magnetic phases for the polarized neutron investigation on POLI, we performed first a non-polarized temperature-dependent neutron diffraction study using the same sample, instrument settings and beam parameters as for the later polarized experiment.

The onset of magnetic ordering was observed about T_N = 30.5 K in accordance with previous studies [6, 13, 14]. Below this temperature the magnetic satellites corresponding to the incommensurate propagation vectors $\boldsymbol{k}_1 = (0.5\ 0\ k_z)$, $\boldsymbol{k}_2 = -\boldsymbol{k}_1 = (0.5\ 0\ -k_z)$, k_z = 0.361(4) appear (Fig. 2). If fitted with one Gaussian peak, the value of k_z increases smoothly from 0.361(1) to 0.3967(1) with temperature decrease from 30.5 K down to ~10 K (Fig. 3a). Below that lock-in temperature the propagation vector component k_z of 0.3967(1) does not change any more down to

4 K. While heating the lock-in value for k_z remain constant up to ~ 20 K showing a significant temperature hysteresis and decrease smoothly with steeper slope toward the higher temperatures, reaching almost the same values as by cooling at about 30 K (Fig. 3a). Hysteretic behavior between cooling and heating in the same temperature region has been reported for the dielectric permittivity in $NdMn_2O_5$ powders [6], which combined with our data suggests a possible coupling between magnetic and electric properties. Fig. 3b shows the temperature evolution of the integrated intensity of the observed magnetic satellite $(2\ 0\ 0)^{-k2}$ fitted by one Gaussian peak while cooling and heating. Slight temperature hysteresis is observable also for the intensity, however in a different temperature region comparing to the thermal evolution of k_z value. The hysteresis is observed between 10 K and 21 K. Above that temperature peak intensity change is perfectly same within cooling or heating. A pronounced change in the slope of the thermal evolution of the magnetic peak intensity is observed at about the same temperature ~ 21 K. This temperature is of special interest as one, where the emergence of the electric polarization in $NdMn_2O_5$ is reported [6]. Similar anomaly in the integrated intensities at ~ 20 K of another magnetic satellites e.g. $(0\ 1\ 0)^{+k1}$, $(2\ 1\ 0)^{-k2}$, $(0\ 0\ 0)^{+k1}$, $(0\ 1\ 2)^{+k2}$ was observed also in the previous studies [6, 13]. In ref. [6] three different types of the magnetic reflections, in the regard to the thermal evolution, were reported: the ones occurring at about 30 K and monotonously increasing down to the lower temperatures e.g. $(0\ 1\ 0)^{+k1}$. Another ones, as mentioned above occurring at about 30 K, slowly increased down to about 20 K and then sharply increasing by lower temperatures. And a third type, which just appears below 20 K and then continuously increase with temperature lowering e.g. $(0\ 0\ 1)^{+k2}$. Such complex behavior has been interpreted as a presence of the different incommensurate magnetic phases with slightly different magnetic propagation vectors k_{z1} and k_{z2} which may coexist in certain temperature regions [6, 13, 14]. The authors of [6, 14] based on the neutron powder diffraction measurements and tiny single crystals proposed a physical picture where between 30 and 15 K an incommensurate phase called ICM1 with coexistence of two slightly different k_{z1} and k_{z2} incommensurate modulations exist and below 15 K those modulations merge into one structure with k_{z2}, called ICM2. The authors of [13] based on the single crystal diffraction suggest the coexistence of the of k_{z1} and k_{z2} incommensurate modulations for all temperatures between 30-2 K, while k_{z1} been dominant magnetic phase in the region 30-20 K and k_{z2} as main magnetic phase at temperatures below ~ 21 K. The presence of the multiple phases with close $\boldsymbol{k}$ vectors should be reflected also in our data. Worth mentioning that hot neutrons single crystal diffractometer is not the best instrument to study the tiny splitting between two magnetic satellites in low-q region, nevertheless optimizing the detector slits-width and monochromator focusing a certain optimization in the resolution may be reached. Fig. 4 shows the temperature dependence of the width of the magnetic satellite $(2\ 0\ 0)^{-k2}$ resulting from the fit with one Gaussian peak while cooling and heating. The resolution limit of the instrument in this setup was of about 0.012 r.l.u. Two main features can be derived from these results. A) Even at low temperature (< 10 K), where it does not change with temperature anymore the absolute value of the peak width fwhm = 0.0168(2) is significantly higher than the resolution of the instrument. This observation is in a good agreement with results reported for powder peaks in [6] and may suggest either broadening of the peak due to some disorder in the magnetic structure or still presence of the two very close k_z structures, as suggested in [13], with only difference, that they should be of the similar magnitude. B) The peak broadening (up to double the instrument resolution limit) is a clear indication for the presence of an additional magnetic phases. Depending on the cooling or heating process, the broadening sets at different temperatures resembling somehow the hysteresis behavior observed for the peaks positions and intensities in (Fig. 3). Close inspection of the high-resolution powder diffraction results from Fig. 6 in Ref. [6] reveals that indeed the primary magnetic phase k_{z1} occurring at about 30 K do not persist down to the very low temperature, but rather down to ~22

K only; then an additional phase with close k_{z2} appears at about 26 K and persist down to ~12 K. This phase can be easily identified by the presence of the 3*k_{z2} modulation in that temperature region only, as it seen at Fig. 6 in Ref. [6]. And finally, at about 21 K a third incommensurate phase with k_{z3} appears, which does not change down to the lowest temperature studied. It is not clear whether results presented in the Fig. 6 of Ref. [6] are measured in the heating or cooling mode, however comparing this physical picture to our results clear similarity to our results in cooling mode could be identified. Thus, in the certain temperature regions different magnetic phases may coexist, like k_{z1} and k_{z2} between 27 - 23 K and k_{z2} and k_{z3} between 26 - 11 K by cooling, leading to the observed peak broadenings. The observed hysteresis in this scenario may be related to the formation of the intermediate k_{z2} structure. While cooling Mn magnetic sub-lattice, which orders at higher temperatures, influences in some way (polarizes) the Nd magnetic sub-lattice. That results in the non-sinusoidal modulated structure k_{z2} and another modulation k_{z3}. At temperatures close to 5 K Nd orders spontaneously resulting in the independent magnetic order with commensurate propagation vector $\boldsymbol{k}_{Nd}$ = (1/2 0 0) in good agreement with previous results [6, 14]. Fig. 5 shows the observed temperature dependence of magnetic peak (2 0 0)$^{+\boldsymbol{k}Nd}$. Both Mn magnetic sublattice with k_{z3} and Nd sublattice with $\boldsymbol{k}_{Nd}$ coexist at temperatures below 5 K. While heating an inverse process of the magnetic influencing may be suggested: the Nd ordered subsystem "polarizes" the Mn sub-lattice in the way that k_{z3} is maintained up to the higher temperatures and intermediate k_{z2} phase occurs later and disappears quicker by heating toward k_{z1} phase. This scenario well resembles the observed in Fig. 3 slow change of the k_z while cooling and steep change while heating. The same model is applicable to the consideration of the peak width evolution at Fig. 4, denoting some "flexibility" in the occurrence of the phase k_{z2} depending on cooling or heating sample history. The two transition temperatures for the magnetic ordering of Nd in $NdMn_2O_5$ has been reported recently from the splitting of crystal fields levels [28]. According to this study, at 28 K ground-state Kramers Doublet splits into two sublevels. This splitting sharply increases below ~18 K and reaches a maximum at 4.5 K. Such behaviour resembles fairly well the thermal evolution of the magnetic structure observed within this study in the heating mode, denoting the influence of the magnetic moment on the Nd on the magnetic structure of the Mn sub-lattice.

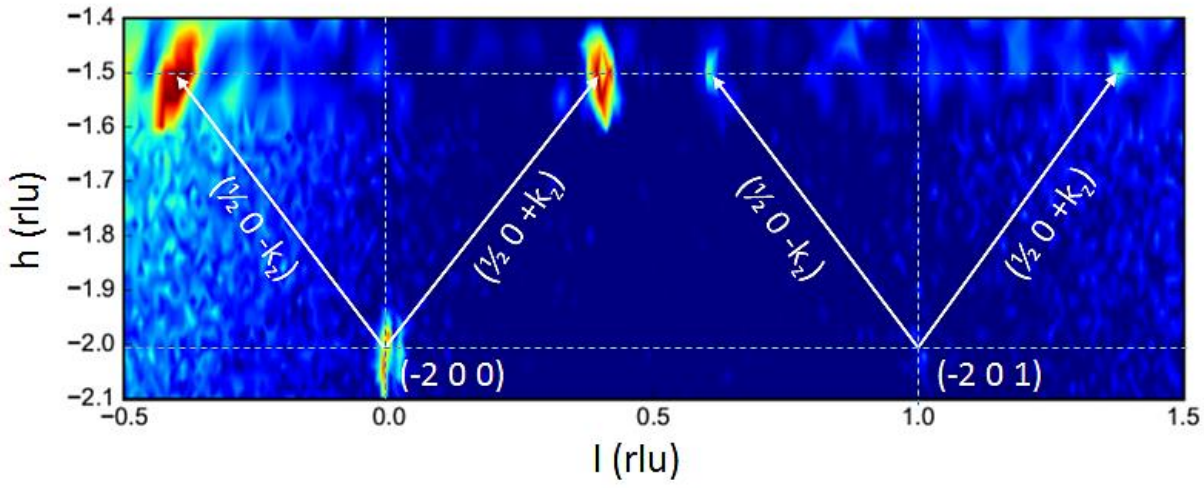

Figure 2: Q-space mapping of incommensurate magnetic Bragg satellites with propagation vectors $\pm\boldsymbol{k}$ = (1/2 0 $\pm k_z$) in $NdMn_2O_5$ at 5 K.

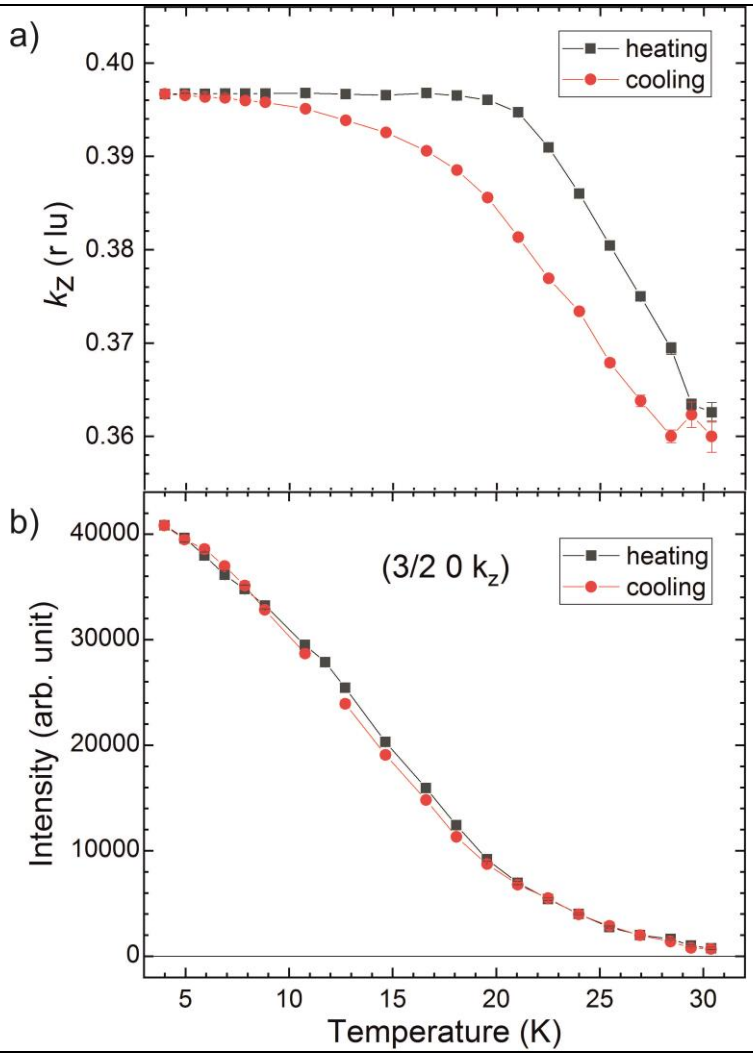

Figure 3: Temperature dependence of: a) the k_z component of magnetic propagation vectors $\boldsymbol{k}_{1,2}$ and b) the integrated intensity of the magnetic reflection $(2\ 0\ 0)^{-\boldsymbol{k}^2}$. Both a) and b) as resulting from the fitting of magnetic reflection with one Gaussian peak. Where not visible, the error bars are smaller than the symbols).

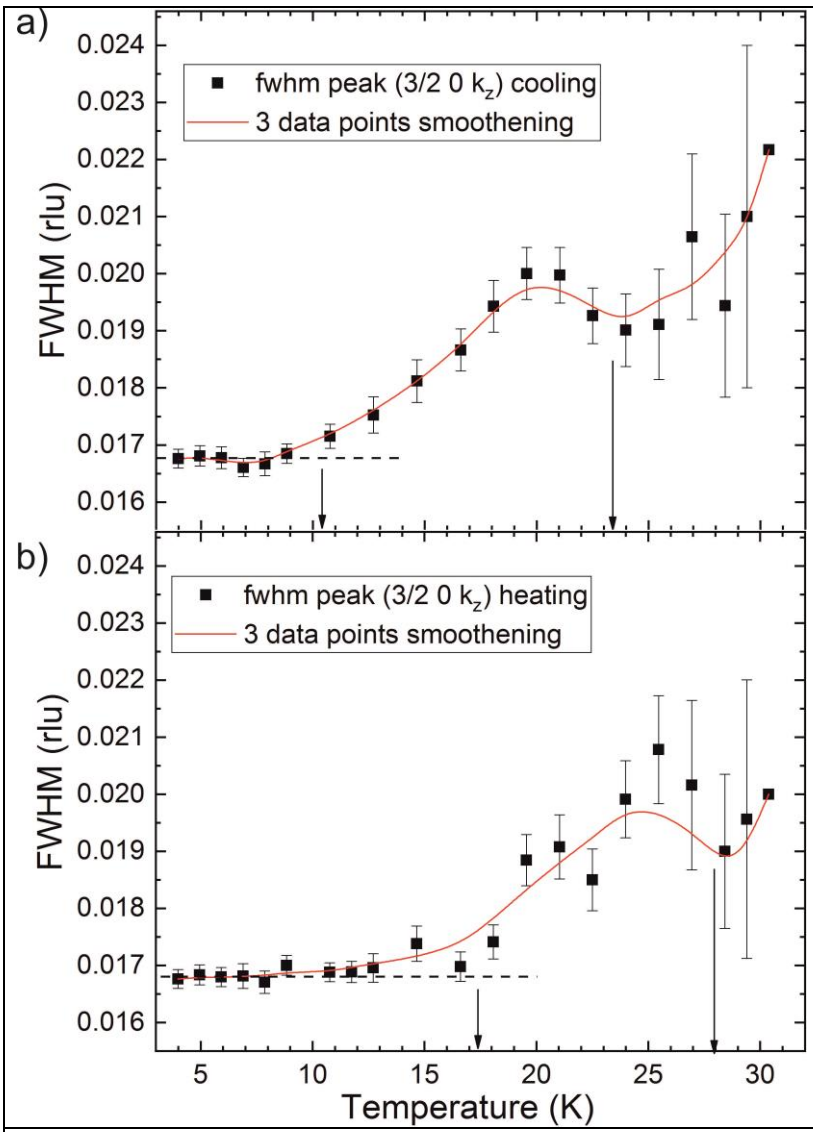

Figure 4: Temperature dependence of the full width at the half maximum (FWHM) for the magnetic Bragg reflection $(2\ 0\ 0)^{-k2}$ as obtained from the fit with one Gaussian peak, a) by cooling and b) by heating. Data points are presented by the black squares, the red lines are the smoothening function by 3 neighboring points applied to the data as a guide to the eyes. The black arrows indicates the temperature region where an "intermediate" magnetic phase with k_{z2} supposed to exist (see main text for more details).

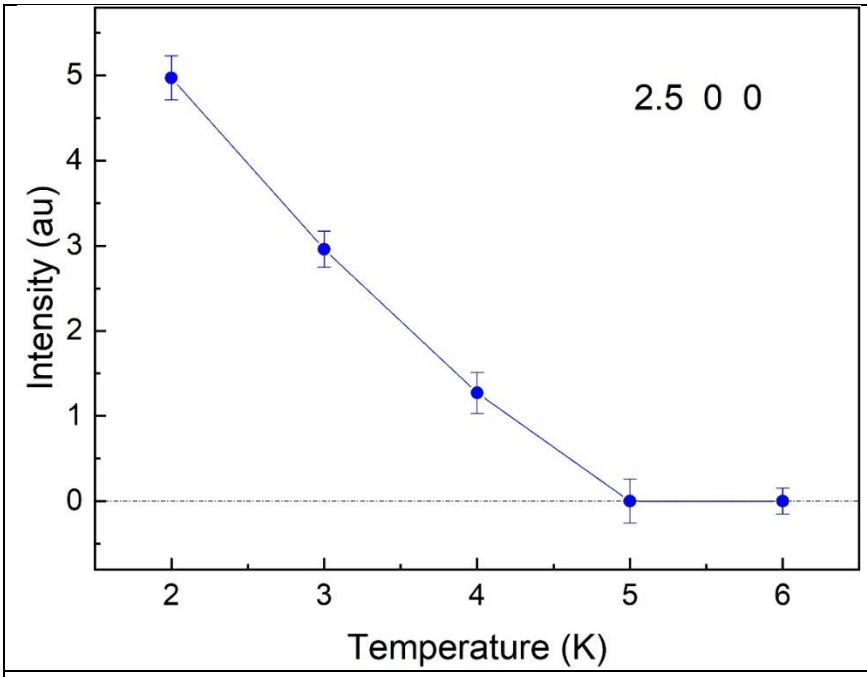

Figure 5: Temperature dependence of the magnetic Bragg reflection (2 0 0)$^{+\boldsymbol{k}^{Nd}}$ by heating with commensurate propagation vector $\boldsymbol{k}_{Nd}$ = (1/2 0 0), associated with spontaneous ordering of the Nd^{3+} magnetic sub-lattice.

C. Magnetic structure in zero electric field by spherical neutron polarimetry

The SNP technique allows to measure the relationship between the polarization of the incident and scattered neutron beams. It allows to distinguish between polarization rotation occurring upon scattering from lattice of the ordered magnetic moments and depolarization due the presence of the magnetic domains. The experimental quantities obtained in SNP experiment for each Bragg reflection are the components P_{ij} of the 3x3 polarization matrix $\boldsymbol{P}$ of the type: $\mathcal{P}_{ij} = \frac{I_{ij}^{+} - I_{ij}^{-}}{I_{ij}^{+} + I_{ij}^{-}}$, where the indices *i, j* refer to one of the orthogonal directions *x*, *y*, *z* of initial and final (scattered from the sample) polarization correspondingly. The first subscript corresponds to the direction of the initial polarization vector, while the second is the direction of analysis. *I* is the measured intensity with polarization parallel "+" and antiparallel "-" to the initial polarization direction *i*. In the general case in all elements $\mathcal{P}_{ij}$ the contributions from nuclear and magnetic scattering exists, some of them containing also nuclear-magnetic interference and chiral scattering terms. A more detailed description of the SNP technique can be found elsewhere [29].

Considering magnetic ordering in crystal as plane elliptical helix, in a general case one can describe it by the following expression:

$$\boldsymbol{M}(\boldsymbol{r}_n) = \boldsymbol{u}\mu_u \cos(\boldsymbol{r}_n \cdot \boldsymbol{k}) + \boldsymbol{v}\mu_v \sin(\boldsymbol{r}_n \cdot \boldsymbol{k}), \qquad (1)$$

where $\boldsymbol{u}, \boldsymbol{v}$ – unit vectors, orthogonal each other, μ_u, μ_v – corresponding amplitudes, $\boldsymbol{r}_n$ – a cell position, helix vector $\boldsymbol{m} = [\boldsymbol{u} \times \boldsymbol{v}]$, and $\boldsymbol{k}$ – helicoid propagation vector. The diffraction on the incommensurate magnetic structure produces pure magnetic reflections, free from nuclear contribution. In the SNP mode we measured only those elements of polarization matrix, which will give most valuable information in a case of incommensurate magnetic structure, namely elliptic parameters $\mathcal{P}_{yy}$ and $\mathcal{P}_{zz}$ and chiral parameters $\mathcal{P}_{yx}$ and $\mathcal{P}_{zx}$ as well as scaling parameter

$\mathcal{P}_{xx}$, denoting total magnetic scattering, which should be equal to -1 for purely magnetic reflection [29]. In this case terms of interest can be expressed as [19]:

$$\mathcal{P}_{yy} = -\mathcal{P}_{zz} \sim \frac{\mu_u{}^2 cos^2\beta - \mu_v{}^2}{\mu_u{}^2 cos^2\beta + \mu_v{}^2} = \frac{R^2 cos^2\beta - 1}{R^2 cos^2\beta + 1} \quad (2)$$

$$\mathcal{P}_{yx} = \mathcal{P}_{zx} \sim \frac{2(1-2n_r)\mu_u\mu_v}{\mu_u{}^2 + \mu_v{}^2} = \frac{2(1-2n_r)Rcos\beta}{R^2 cos^2\beta + 1} \quad (3)$$

In these expressions $\boldsymbol{v}$ considered to be directed vertically, $\boldsymbol{u}$ - horizontally, β is angle between helix vector $\boldsymbol{m}$ and scattering vector $\boldsymbol{q}$ (Fig. 6), $R = \mu_u/\mu_v$ - ellipticity, n_r – portion of "right-hand" helices in crystal, $n_l = 1 - n_r$ is a portion of "left-hand" helices. Thus, the overall relative chirality for the k_n structure could be denoted as: $Ck_n = n_l(k_n) - n_r(k_n)$.

It should be noted, that because of low intensities of scattering from phase k_{z1} and k_{z2} above 22 K (Fig. 3b) the measurements of polarization matrix elements were performed only for satellites from phase k_{z3} at 4 K and later at 18 and 20 K in heating mode in order to observe any influence of the k_{z2} phase (правильно ли? т.е . измерить для того, чтобы наблюдать влияние k_{z2} phase?). The measured polarization matrix elements for two different magnetic Bragg satellites with $+\boldsymbol{k}$ and $-\boldsymbol{k}$ vectors and different angles β (see Fig. 6) measured at 4 K, 18 K and 20 K are shown in Table II.

Table II. Polarization matrix elements for magnetic satellites $(2\ 0\ 0)^{-\boldsymbol{k}2}$ and $(0\ 0\ 0)^{+\boldsymbol{k}1}$ measured at different temperatures and zero electric filed.

4 K		$(2\ 0\ 0)^{-\boldsymbol{k}2}$			$(0\ 0\ 0)^{+\boldsymbol{k}1}$	
	x	y	z	x	y	z
x	-1.041(14)			-0.98(4)		
y	-0.19(5)	-0.316(13)		-0.20(2)	-0.20(2)	
z	-0.08(4)		0.292(14)	-0.19(2)		0.19(2)
18 K		$(2\ 0\ 0)^{-\boldsymbol{k}2}$			$(0\ 0\ 0)^{+\boldsymbol{k}1}$	
	x	y	z	x	y	z
x	-0.98(7)			-0.98(10)		
y	-0.05(7)	-0.580(22)		-0.19(5)	0.35(2)	
z	-0.09(6)		0.584(24)	-0.06(5)		-0.36(2)
20 K		$(2\ 0\ 0)^{-\boldsymbol{k}2}$			$(0\ 0\ 0)^{+\boldsymbol{k}1}$	
	x	y	z	x	y	z
x	-1.036(23)			-0.98(7)		
y		-0.728(21)				
z			0.721(21)			-0.53(10)

The presence of the non-zero chiral parameters $\mathcal{P}_{yx}$ and $\mathcal{P}_{zx}$ of the same sign is a clear direct evidence that underlying incommensurate magnetic structure at 4 K is of the chiral type (cycloidal or helical order) and not a flat spin wave modulation as previously suggested [6]. The non-zero value of these components gives an evidence about non-equal population of the domains with "right" and "left" chiral handedness. Using the data at 4 K from Table I the calculation gives an estimation for chirality in k_{z3} phase Ck_{z3} = 0.20(2). At 18 K one still observes some non-zero chiral terms, but statistics is not as good because of the low satellite intensity in comparison to the 4 K. However, the fact, that both $\mathcal{P}_{yx}$ and $\mathcal{P}_{zx}$ components are of the same sign for both reflections and their sign is same as for 4 K, may serve as an indication that at 18 K the chiral magnetic phase k_{z3} is still persisting also keeping the same type unbalance between two different chiral handedness. At 20 K the chiral components $\mathcal{P}_{yx}$ and $\mathcal{P}_{zx}$ could not be measured any more reliably. This can't be explained solely by decreasing statistics, and is an intrinsic treasure of the changing magnetic structure.

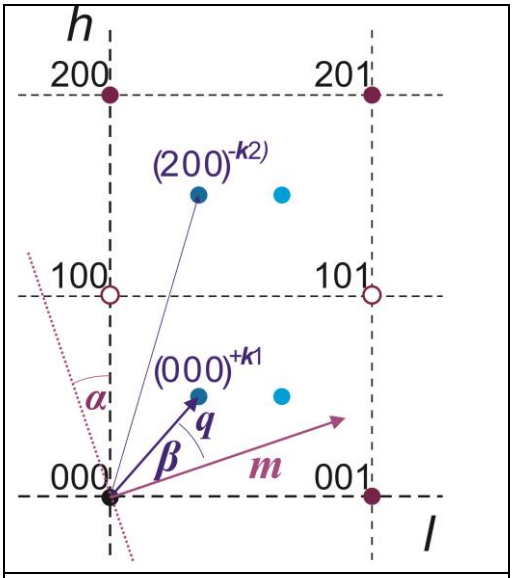

Figure 6. Scheme of the consideration of directions in reciprocal space

The elliptic parameters $\mathcal{P}_{yy}$ and $\mathcal{P}_{zz}$ for both (2 0 0)$^{-k2}$ and (0 0 0)$^{+k1}$ reflections in Table I also changes with temperature. The more pronounced effect takes place for (0 0 0)$^{+k1}$ satellite, where $\mathcal{P}_{yy}$ and $\mathcal{P}_{zz}$ change their signs between 4 K and 18 K. This is clear evidence that orientation of the magnetic moments in k_{z3} structure changes significantly between those temperatures while heating. Comparing this result with the temperature evolution of the peak width from Fig. 4b, this reorientation may be ascribe to the emerging additional phase called k_{z2} at an intermediate temperature. No orientation change is observable between 18 and 20 K by further temperature increase. Assuming helical type magnetic structure and using Eq. (2) it is possible to calculate resulting magnetic helix parameters like ellipticity *R* and helix plane orientation. Obtained in this way angle α between magnetic helix plane and crystallographic *ab* plane for the k_{z3} magnetic structure is: 22.2(3.2)° at 4 K. At higher temperatures helix changes its orientation: the major and minor elliptic axes are swept and the angle between the helix plane to the *ab* plane is tilted to the α = -4.7(4)° at 18 K, and α= -10.4(1.2)° at 20 K respectively. Ellipticity of the magnetic structure *R*, denoting the ratio between major and minor axis of the helix in the plane, changes also with temperature. *R* = 1 would correspond to a perfectly circular helix. Deviations from 1 denotes distortions (elongations) of the ellipse. Calculated for different temperatures *R* values are: 0.77(13), 2.16(11), 3.06(50) for 4, 18, and 20 K respectively, showing clear shrinking (elongation) of the helix toward the transition temperature around 21 K, where the chiral character is disappeared (as shown in the next chapter), and plane spin density wave modulation is formed. The schematic representation of such transformation from chiral helical structure to non-chiral collinear spin-wave one is shown at Fig. 7.

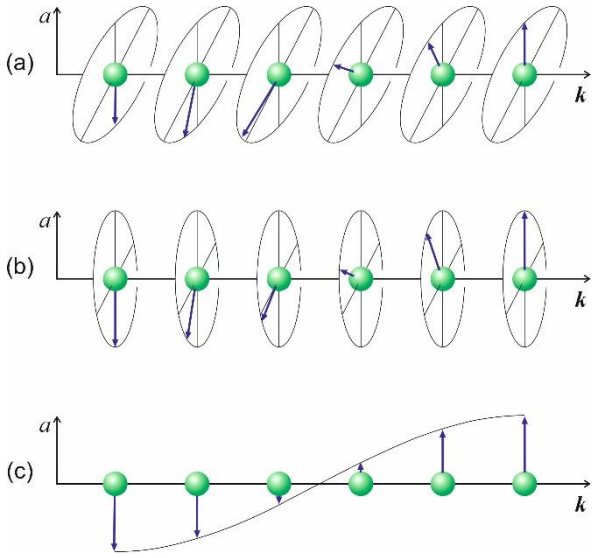

Figure 7. Schematic representation of the transformation of an elliptical spiral into a transverse spin-wave modulation in $NdMn_2O_5$ with temperature increase: (a) almost circular helix with minor axis along *a* – corresponding to configuration at 4 K, (b) – transformed (elongated) helix with major axis along *a* at 18-20 K, and (c) – plane spin wave modulation presumably at $T > 21$ K.

D. Magnetic chirality under applied electric field by polarized neutron diffraction

Because of low intensities of magnetic satellites, for the study of electric field dependence on chiral scattering, in order to increase statistics, we applied the technique of polarized neutron diffraction without analysis of scattered beam polarization. In this case the loss of neutrons due to the limited transmission of the analyzer is avoided, while chiral scattering can be unambiguously detected. The expression for the intensity of polarized neutrons, scattered on a magnetic satellite from helical structure [30], can be written in the simplified form as:

$$I_{\boldsymbol{x}}^{\pm} \sim \boldsymbol{M}_{\perp}\boldsymbol{M}_{\perp}^{*} \mp iCk_n \left(\boldsymbol{M}_{\perp} \times \boldsymbol{M}_{\perp}^{*}\right)_x \qquad (4)$$

where $\boldsymbol{M}_{\perp}$ – effective magnetic moment, participated in scattering process, perpendicular to scattering vector ***q:***

$$\boldsymbol{M}_{\perp} = \boldsymbol{q} \times (\boldsymbol{M} \times \boldsymbol{q}) \qquad (5)$$

and $I_{\boldsymbol{x}}^{\pm}$ - intensity of scattered neutrons with initial neutron polarization along ***x***-axis (+) or opposite to it (-) and ***x***-axis is directed along the scattering vector ***q***. In this way, total magnetic intensity $I_M = (I_x^+ + I_x^-)/2$ as well as pure chiral part of the magnetic scattering $I_{Ch} = (I_x^+ - I_x^-)/2$ can be obtained if $Ck_n \neq 0$. At the temperature 4 K the results for chirality obtained by this technique were compared with those from SNP for the consistency.

Temperature evolution of chiral scattering, measured on magnetic satellite $(2\ 0\ 0)^{-k2}$ without electric field is shown in Fig. 8a. It is easy to observe, that the chiral scattering appears below $T \approx$

21 K. This means that below $T_N \approx 30$ K in $NdMn_2O_5$ a non-chiral incommensurate magnetic ordering emerges, while at $T_{Ch} \approx 21$ K the transition to chiral structure takes place. The crossover observed in the temperature dependence of the integrated intensities of magnetic satellites reflect this transition and proposed k_{z3} magnetic structure is of chiral nature. The existence of the non-chiral spin wave modulation phase in the intermediate temperature region between paramagnetic and ferroelectric phases is observed also for type-II multiferroic compounds – members of perovskite manganites family $RMnO_3$ with R = Tb, Dy [31-33] as well as some doped RMn_2O_5 family representatives like $YMn^{4+}(Mn_{0.88}Ga_{0.12})^{3+}O_5$ [18].

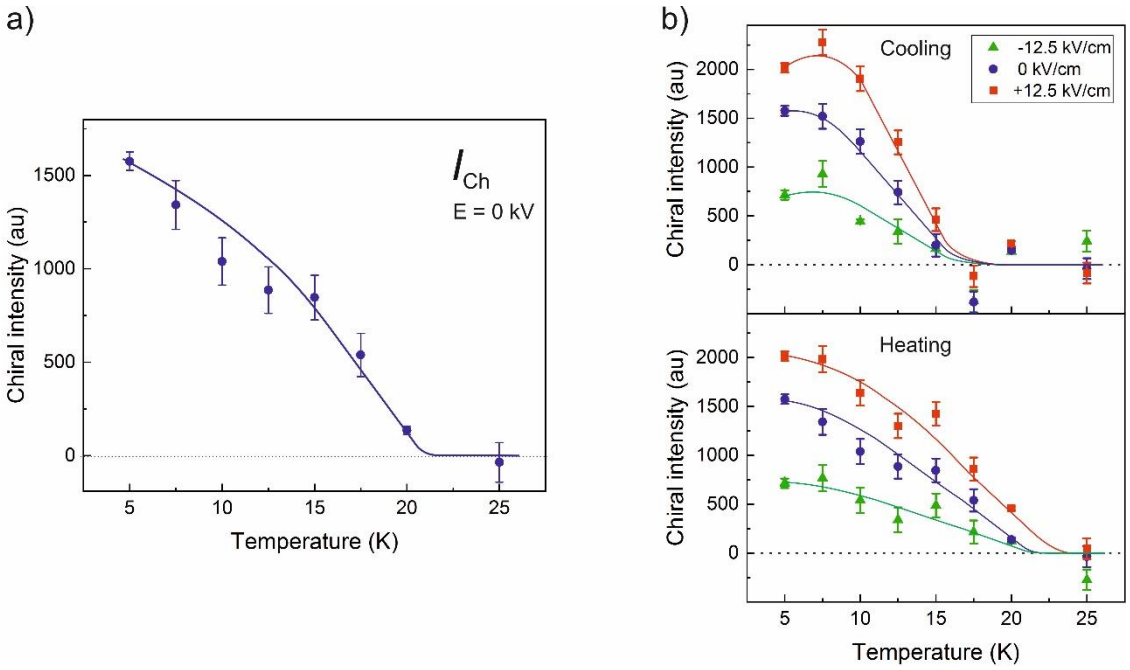

Figure 8. a) Temperature evolution of chiral scattering I_{Ch}, measured on satellite $(2\ 0\ 0)^{-k2}$ in heating mode without electric field. b) The temperature evolution of chiral scattering I_{Ch} on the same satellite as function of electric field on cooling and heating mode. Solid lines are guides to eyes.

In order to study the effect of electric field on the magnetic properties of $NdMn_2O_5$ we first applied +5 kV voltage along *b* direction (which yields electric field +12.5 kV/cm) at fixed low temperature of 4 K while sample was cooled without electric field (ZFC). This action had no measurable effect on the magnetic satellites. Then the measurements in field cooled (FC) mode were performed in the following way: crystal was warmed up to the temperature of 40 K, i.e. well above the transition temperature T_N = 30.5 K, then the voltage was applied and sample cooled down to 5 K under applied electric field. The sample was warmed up back to 40 K under the same field, then the voltage value was changed. The following sequence of applied fields was used: +5 kV (+12.5 kV/cm), +2.5 kV (+6.25 kV/cm), 0 kV, -2.5 kV (-6.25 kV/cm), -5 kV (-12.5 kV/cm). The intensities I_x^+ and I_x^- were measured for selected magnetic satellites while cooling/heating under field at temperatures of 25 K, 20 K and then with 2.5 K step by temperature lowering down to 5 K, and then while heating at the same temperature points. The results of such measurements for satellite $(2\ 0\ 0)^{-k2}$ are presented on Fig. 8b. The application of electric field in FC mode do not change T_{Ch} for the same cooling/heating mode, while intensity of the chiral scattering changes considerably. Depending on the field polarity certain chiral domains will be favorited or suppressed. The behavior seems to be symmetric in regard to the pre-existed in the sample unbalance between the domains with two handedness at zero field. Some temperature hysteresis of few Kelvin for T_{ch} around 20 K depending on the heating or cooling mode was observed for chiral scattering. One should point out that the application of electric field (FC mode) didn't change elliptic terms within accuracy of the measurements. In the Fig. 9 the chirality Ck_3 is plotted as function of applied electric field. Pretty much linear behavior is observable for the both phases. This is different comparing to the situation observed in $TbMn_2O_5$ [19], where similar measurements reveal a kind of hysteretic behavior in the chirality vs. electric field phase diagram. This result denotes weaker pinning of the chiral domain walls to the crystal frame in $NdMn_2O_5$, than in the case of $TbMn_2O_5$.

IV. DISCUSSION

The emergence of the chiral scattering was observed at the temperature T_{Ch} which coincides with T_{CE} where ferroelectric polarization starts to occur. This leads us to the suggestion, that namely the chiral magnetic structure is the origin of the ferroelectric polarization in $NdMn_2O_5$. Here it is appropriate to mention that antisymmetric DMI determines the direction of rotation of the spirals in the chiral magnetic structures [20]. The possibility of the existence of non-zero integral DMI in RMn_2O_5 was discussed previously in YMn_2O_5 [18] and recently for $TbMn_2O_5$ [19]. The considerations use a qualitative model based on the antisymmetric super-exchange through an anion [34, 35] taking into account for the crystal symmetry of non-centrosymmetric space group *Pm* rather than *Pbam* [11]. Apparently, the

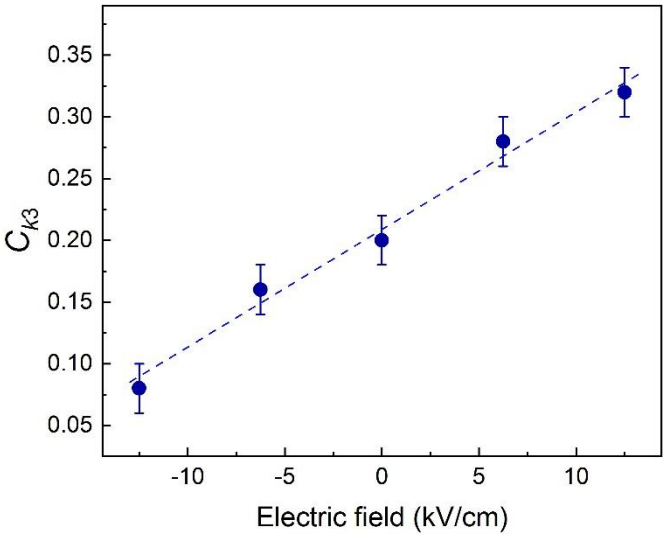

Figure 9. Electric field dependence of magnetic chirality Ck_3 measured at 4 K in FC mode.

argumentation made there for $TbMn_2O_5$ is applicable also for $NdMn_2O_5$, which we repeat briefly here.

The antisymmetric super-exchange through an anion can be expressed as [34, 35]:

$$V_{DM}=d(\theta)[\mathbf{R}_1\times\mathbf{R}_2][\mathbf{S}_1\times\mathbf{S}_2], \quad (5)$$

$\boldsymbol{D} = d(\theta)[\mathbf{R}_1\times\mathbf{R}_2]$ is Dzialoshinsky vector in this case. $\mathbf{R}_1$, $\mathbf{R}_2$ are unit vectors, connecting magnetic ions with anion. Their vector product fixes the direction of $\boldsymbol{D}$. The antisymmetric exchange parameter $d(\theta)$ depends in a rather complex manner on the local anisotropy of metal ion, on the particularities of metal-ligand bonds and its sign depends on the bond angle θ [32]. The sign of the antisymmetric parameter $d(\theta)$ changes at a critical angle θ_k which is characteristic for each particular interacting cation-anion group. Within monoclinic space group *Pm* [11] the four pairs of interacting manganese ions Mn^{3+} - Mn^{4+} will give non-zero total interacting vector $\boldsymbol{D}$ (Fig. 10). For these pairs Heisenberg exchange interactions usually considered as J_3 and J_4. By the analogy, we will designate antisymmetric interactions under consideration as $\boldsymbol{D}_3$ and $\boldsymbol{D}_4$. In the case of non-centrosymmetric space group *Pm* there will be four inequivalent interaction $\boldsymbol{D}_{31}$, $\boldsymbol{D}_{32}$ and $\boldsymbol{D}_{41}$, $\boldsymbol{D}_{42}$. The bond angles on the regarded exchange paths are close to 130°, which is a critical super-exchange value according to Goodenough-Kanamori-Andersen rules [36].

It was shown for RMn_2O_5 [37] that oxygen locations relative to those of Mn^{3+} and Mn^{4+} ions play important role in the determination of the magnetic properties. In this situation, tiny deviation in anion position could cause a sharp change of the magnetic interaction [37]. This change should refer not only to the symmetrical exchange but to antisymmetric one as well. The comparison of the exchange bonds between the manganese ions as shown in Fig. 10 for $NdMn_2O_5$ and $TbMn_2O_5$ can be done based on the *Pbam* crystal structure, since, to our best knowledge, there is no exact data on the oxygen positions in $NdMn_2O_5$ and $TbMn_2O_5$ within space group *Pm* available. According to data from Ref. [7] the Mn11 – O43 – Mn23 and Mn11 – O44 – Mn24 angles and bonds corresponding to $\boldsymbol{D}_{41}$, $\boldsymbol{D}_{42}$ are similar for the both compounds. Whereas, for the pairs Mn11 – O31 – Mn21 and Mn11 – O32 – Mn22 (defining $\boldsymbol{D}_{31}$, $\boldsymbol{D}_{32}$) they are different. In $NdMn_2O_5$ there is noticeable displacement of the oxygen ions O31, O32 away from the Mn11 (Mn^{4+}) toward the ions Mn21 and Mn22 (Mn^{3+}) respectively, comparing to $TbMn_2O_5$. The bond length Mn1-O3 is 2.076 Å for $NdMn_2O_5$ and 2.021 Å for $TbMn_2O_5$ respectively [7]. In both cases the angles are very close to the critical value of 132.4-132.5°.

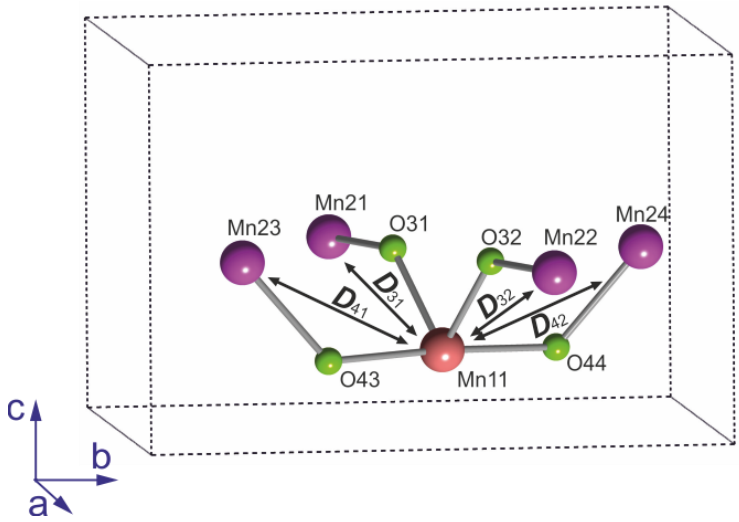

Figure 10. Exchange paths for Mn^{4+} - Mn^{3+} pairs in RMn_2O_5 considering monoclinic space group *Pm*.

Comparing the positions for the oxygen ions, for space group *Pm* [11] with those for *Pbam* [7] one can see that oxygen ions involved in DM interaction under our consideration O31, O32, O43, O44 have the largest polar displacements. Being the most "mobile" in this structure, these ions (or some of them) could undergo displacements under the influence of the electric field. These displacements provoke the change in the sign of the antisymmetric exchange parameter $d(\theta)$ in some

domains, thus favoring predominant formation of the domains with certain handedness of the helices.

According to the obtained results of the chirality evolution under applied electrical field we can suppose, that geometrical arrangement of the considered super-exchange in $NdMn_2O_5$ is closer to the critical one than that of $TbMn_2O_5$, and therefore $NdMn_2O_5$ demonstrates less rigid chirality-to-lattice coupling. Crystal structure of RMn_2O_5 provides multiple competing magnetic interactions, and correspondingly it is exchange frustrated, which yields the competing magnetic ground states. For rare earth ions with ion radius lower than that of Nd^{3+} ground state with commensurate structure, characterized by $\boldsymbol{k}$ = (0.5 0 0.25) becomes favorable in some temperature region, which is not the case for $NdMn_2O_5$. At the same time the spiral spin structure is still preserved in this commensurate phase in such compounds [19, 38]. Therefore, it is reasonable to assume, that even in the in commensurate magnetic phase DMI interaction continue to persist and manifests in a considerable way generating weak ferroelectric polarization. The latter may be enhanced by some another mechanism, such as e.g. exchange striction [12] or/and oxygen spin polarization [39].

The $NdMn_2O_5$ system demonstrates ability to generate ordered magnetic phases with slightly different $\boldsymbol{k}$-vectors depending on the temperature. Much the same situation associated with the coexistence of several magnetic phases with similar wave vectors was observed also in $DyMn_2O_5$ [40]. Such a state can be realized due to the presence of several competing magnetic states. It was shown in [40] that the choice of the ground state can be obtained by a relatively small magnetic field, which reflects the proximity in energy of the competing ground states in RMn_2O_5. In the case of $NdMn_2O_5$, the observed coexistence of magnetic phases can be associated with the choice of the different ground states occurring due to a subtle deviations in the local environment of the manganese subsystem. Such a discrete splitting of the crystal field levels of the 4f electrons in Nd^{3+} ions in $NdMn_2O_5$ under the studied here temperatures has been recently experimentally demonstrated by the infrared spectroscopy [28].

V. SUMMARY

Detailed investigation of the complex incommensurate magnetic ordering in large single crystals of $NdMn_2O_5$ has been performed using polarized and non-polarized neutron diffraction methods. Below T_N = 30.5 K a transition to the incommensurate magnetic order (most probably plane spin density wave modulation) with propagation vectors $\boldsymbol{k}_1 = (0.5\ 0\ k_z)$, $\boldsymbol{k}_2 = -\boldsymbol{k}_1 = (0.5\ 0\ -k_z)$ with k_{z1} = 0.361(4) takes place. A few degrees below, at $T \approx 27$ K an additional incommensurate magnetic phase with similar propagation vectors k_{z2} occurs. This phase, however, show strong deviation from sinusoidal modulation as confirmed by the observation of the $3*k_{z2}$ modulations [6]. Interestingly that just at the same temperature an independent study of the CF energy levels of Nd^{3+} reports the splitting of the ground-state Kramers doublet two sublevels [28], demonstrating a kind of "magnetic polarisation" of the Nd ions by the Mn magnetic sub-lattice. Thus, distorted k_{z2} modulation may be attributed to the magnetisation of Nd sublattice. This magnetic phase seems to disappear, when the new chiral magnetic phase called k_{z3} at lower temperature is fully formed. Significant temperature hysteresis is observed in the formation of the k_{z2} and k_{z3} phases depending on the heating or cooling sample history. Reported here results are obtained using larger crystal of high quality and modern instrumentation with improved resolution and neutron flux in comparison to the previous studies [6,13,14] reporting somehow contradictory results about thermal evolution of incommensurate order in $NdMn_2O_5$. Our new findings allow unifying those results, and concluding, that system demonstrates ability to generate magnetic ordered phases of different types at temperatures between 30 and 4 K. According to the SNP measurements, below $T_{Ch} \approx 21$ K magnetic structure of $NdMn_2O_5$ becomes chiral and this kind of magnetic order is associated

with the occurrence of the weak ferroelectricity. The resulting at lower temperature k_{z3} magnetic structure could be well approximated using general elliptic helix model. Characteristic parameters of the helix, like ellipticity (ratio between minor and major ellipse axis) and inclination of the helix plane in regard to the crystallographic *ab* plane could be calculated for different temperatures. It was shown, that while heating between 4 and 18 K a reorientation transition of the helical order (interchange between the minor and major axis orientation and change in the sigh on the inclination angle) happens. This reorientation may be caused by the occurrence of the k_{z2} phase attributed to the partial magnetic ordering of the Nd ions at this temperature range observed in recent work [28]. Below ~ 5 K a commensurate AFM order with propagation vector (1/2 0 0) is formed on Nd, this coexists with incommensurate structure k_{z3}. It is worth noting, that we did not perform explicit investigations of the magnetic ordering on Nd within this study. With temperature increase toward T_{Ch}, magnetic ellipse on Mn becomes more stretched along *a*-axis. The difference in the population of the "right" and "left" handedness domains in the chiral magnetic phase was observed in as-grown crystal. This difference can be controlled by the external electric field in field cooled mode. Linear dependence of the magnetic chirality from the applied electric field strength was observed within the used field region of ±12.5 kV/cm. Thus, strong magneto-electric coupling for $NdMn_2O_5$ was demonstrated experimentally for the first time. The results are qualitatively discussed within frame of antisymmetric DMI super-exchange. Concluding for more general case, that integral antisymmetric DM exchange may exist in RMn_2O_5 manganates for the structures with the symmetry lower than *Pbam*. Our experimental findings are in a good agreement with the suggestion that DMI mechanism can be responsible for the emergence of weak ferroelectricity in RMn_2O_5 multiferroics family where weak ferroelectric phase is observed simultaneously with incommensurate magnetic chiral structure.

ACKNOWLEDGMENTS

The authors are grateful to S.V. Gavrilov for technical assistance and to S.V. Maleyev for fruitful discussions. This work is supported by Russian Foundation for Basic Research grant No. 16-02-00545-a. The work is based on the results obtained on instrument POLI, operated by RWTH Aachen in cooperation with FZ Juelich (Juelich-Aachen Research Alliance JARA).

---

[1] N. Hur, S. Park, P. A. Sharma, J. S. Ahn, S. Guha, S. W. Cheong. Nature **429**, 392 (2004).
[2] Y. Noda, H. Kimura, M. Fukunaga, S. Kobayashi, I. Kagomiya, K. Kohn. J. Phys.: Condens. Matter **20**, 434206 (2008).
[3] G. R. Blake, L. C. Chapon, P. G. Radaelli, S. Park, N. Hur, S. W. Cheong, J. Rodriguez-Carvajal. Phys. Rev. B **71**, 214402 (2005).
[4] M. Fukunaga, Y. Sakamoto, H. Kimura, Y. Noda, N. Abe, K. Taniguchi, T. Arima, S. Wakimoto, M. Takeda, K. Kakurai, K. Kohn. Phys. Rev. Lett. **103**, 077204 (2009).
[5] P. G. Radaelli L. C. Chapon, A. Daoud-Aladine, C. Vecchini, P. J. Brown, T. Chatterji, S. Park, S.-W. Cheong. Phys. Rev. Lett. **101**, 067205 (2008).
[6] S. Chattopadhyay, V. Baledent, F. Damay, A. Gukasov, E. Moshopoulou, P. Auban-Senzier, C. Pasquier, G. Andre, F. Porcher, E. Elkaim, C. Doubrovsky, M. Greenblatt, P. Foury-Leylekian. Phys. Rev. B **93**, 104406 (2016).
[7] J. A. Alonso, M. T. Casais, M. J. Martínez-Lope, J. L. Martínez, M. T. Fernañdez-Díaz. J. Phys.: Condens. Matter **9**, 8515 (1997).
[8] V. Polyakov, V. Plakhty, M. Bonnet, P. Burlet, L.-P. Regnault, S. Gavrilov, I. Zobkalo, O. Smirnov. Physica B **297**, 2008 (2001).

[9] I. Kagomia, S. Matsumoto, K. Kohn, Y. Fukuda, T. Shoubu, H. Kimura, Y. Nida, N. Ikeda. Ferroelectrics **286**, 167 (2003).
[10] L.C. Chapon, G.R. Blake, M.J. Gutmann, S. Park, H. Hur, P.G. Radaelli, S.-W. Cheong, Phys. Rev. Lett. **93**, 177402 (2004).
[11] V. Baledent, S. Chattopadhyay, P. Fertey, M.B. Lepetit, M. Greenblatt, B. Wanklyn, F.O. Saouma, J.I. Jang, P. Foury-Leylekian. Phys. Rev. Lett. **114**, 117601 (2015).
[12] P.G. Radaelli, L.C. Chapon. J. Phys.: Condens. Matter **20**, 434213 (2008).
[13] I. A. Zobkalo, S. V. Gavrilov, N. Z. Saw Nyi, S. N. Barilo, S. V. Shiryaev. J. Magn. Magn. Mater. **354**, 85 (2014).
[14] S. Chattopadhyay, V. Balédent, P. Auban-Senzier, C. Pasquier, C. Doubrovsky, M. Greenblatt, P. Foury-Leylekian. Physica B **460**, 214 (2015).
[15] H. Katsura, N. Nagaosa, V. Balatsky, Phys. Rev. Lett. **95**, 057205 (2005).
[16] I. A. Sergienko, E. Dagotto, Phys. Rev. B **73**, 094434 (2006).
[17] M. Fukunaga, Y. Noda. J. Phys. Soc. Jpn. **79**, 054705 (2010).
[18] S. Wakimoto, H. Kimura, Y. Sakamoto, M. Fukunaga, Y. Noda, M. Takeda, K. Kakurai. Phys. Rev. B **88**, 140403 (2013).
[19] I.A. Zobkalo, S.V. Gavrilov, A. Sazonov, V. Hutanu. J. Phys.: Condens. Matter **30**, 205804 (2018).
[20] S.V. Maleyev. Physica B **350**, 26 (2004).
[21] S.V. Shiryaev, G. L. Bychkov, S. N. Barilo. D. D. Khalyavin, A. G. Soldatov, Yu. G. Pashkevich. Proc. of 4-th Int. Conf. Single Crystal Growth & Heat and Mass Transfer, Editor V. P. Ginkin, Obninsk, Russia, Sept.24-28, 2001, v.1, 251 (2001).
[22] B. Pedersen, Journal of large-scale research facilities **1**, A4 (2015).
http://dx.doi.org/10.17815/jlsrf-1-23
[23] V. Huţanu, M. Meven, E. Lelièvre-Berna, G. Heger, Physica B 404 2633–2636 (2009)
[24] V. Hutanu, Journal of large-scale research facilities **1**, A16 (2015).
http://dx.doi.org/10.17815/jlsrf-1-22
[25] V. Hutanu, W. Luberstetter, E. Bourgeat-Lami, M. Meven, A. Sazonov, A. Steffen, G. Heger, G. Roth, and E. Lelièvre-Berna, Rev. Sci. Instrum. **87**, 105108 (2016).
[26] V. Hutanu, M. Meven, S. Masalovich, G. Heger, and G. Roth. J. Phys.: Conf. Series **294**, 012012 (2011).
[27] J. Rodriguez-Carvajal, Physica B **192**, 55 (1993).
[28] S. Mansouri, S. Jandl, M. Balli, P. Fournier, B. Roberge, M. Orlita, I.A. Zobkalo, S.N. Barilo, S.V. Shiryaev. Phys. Rev. B **98**, 205119 (2018).
[29] P. J. Brown and T. Chatterji, *Neutron Scattering from Magnetic Materials* (Elsevier Science, Amsterdam, 2006), pp. 215–244.
[30] Yu. A. Izyumov and R. P. Ozerov, *Magnetic Neutron Diffraction* (Nauka, Moscow, 1966; Plenum, New York, 1970).
[31] M. Kenzelmann, A. Harris, S. Jonas, C. Broholm, J. Schefer, S. Kim, C. Zhang, S. W. Cheong, O. Vajk, J. Lynn. Phys. Rev. Lett. **95** 087206 **(**2005).
[32] T. Arima, A. Tokunaga, T. Goto, H. Kimura, Y. Noda and Y.Tokura. Phys. Rev. Lett. **96**, 097202 (2006).
[33] O. Prokhnenko, R. Feyerherm, E. Dudzik, S. Landsgesell, N. Aliouane, L. C. Chapon, D. N. Argyriou. PRL **98,** 057206 (2007).
[34] F. Keffer. Phys. Rev. **126,** 896 (1962).
[35] A. S. Moskvin, I. G. Bostrem. Sov. Phys. Solid State **19,** 1532 (1977).
[36] P.W. Anderson, in *Magnetism*, edited by G.T. Rado and H. Suhl (Academic Press, New York, 1963), Chap. 2, pp. 25-83.
[37] L. M. Volkova, D. V. Marinin. J. Phys.: Condens. Matter **21,** 015903 (2009).

[38] H. Kimura, S. Kobayashi, Y. Fukuda, T. Osawa, Y. Kamad, Y. Noda, I. Kagomiya, K. Kohn J. Phys. Soc. Jpn. **76,** 074710 (2007).
[39] T. A. W. Beale, S. B. Wilkins, R. D. Johnson, S. R. Bland, Y. Joly, T. R. Forrest, D. F. McMorrow, F. Yakhou, D. Prabhakaran, A. T. Boothroyd, P. D. Hatton. Phys. Rev. Lett. **105** 087203 (2010).
[40] W. Ratcliff II, V. Kiryukhin, M. Kenzelmann, S.-H. Lee, R. Erwin, J. Schefer, N. Hur, S. Park, and S-W. Cheong. Phys. Rev. B **72**, 060407(R) (2005).